

# Support motion of a finite bar with an external spring

Journal of Low Frequency Noise,  
Vibration and Active Control  
2022, Vol. 0(0) 1–16  
© The Author(s) 2022  
DOI: 10.1177/14613484221080346  
[journals.sagepub.com/home/lfn](https://journals.sagepub.com/home/lfn)  


Jeng-Tzong Chen<sup>1,2,3,4,5</sup> , Hao-Chen Kao<sup>1</sup>, Ying-Te Lee<sup>1</sup> and Jia-Wei Lee<sup>6</sup>

## Abstract

In this paper, we gave the vibration analysis of a finite bar with an external spring on one side and the support motion on the other side. Two analytical methods, the mode superposition method in conjunction with the quasi-static decomposition method and the method of characteristics using the diamond rule, were employed to solve this problem. Both advantages and disadvantages of two methods were discussed. It is interesting to find that the mode superposition method can capture the silent area in terms of sum of an infinite series while the method of characteristics using the diamond rule can exactly derive the dead zone. Besides, it is found that discontinuities always occur at the location on the characteristic lines. Discussions of direct and inverse problems are also addressed.

## Keywords

Support motion, mode superposition method, quasi-static decomposition, diamond rule

## Introduction

Wave propagation is very important in physics and mechanics because there are various engineering problems which can be modeled by using the wave equation. Many researchers solved this problem by using various methods, for example, the mode superposition technique,<sup>1</sup> the method of separation variables,<sup>2,3</sup> the method of quasi-static decomposition,<sup>3,4</sup> the method of the diamond rule,<sup>3,5</sup> the image method,<sup>5</sup> the finite element method (FEM),<sup>6</sup> the boundary element method (BEM),<sup>7</sup> and the meshless method.<sup>8</sup>

The Rayleigh-damped Bernoulli–Euler beam subjected to multi-support excitation and the string subjected to support motions have been studied by using many methods.<sup>3,4</sup> Mindlin and Goodman<sup>9</sup> proposed the quasi-static decomposition approach. D’Alembert’s solution provides an exact solution. Method of characteristics can be found in the textbook of Farlow.<sup>10</sup> It is widely employed to solve various kinds of problems, for example, water hammer.<sup>11</sup> The diamond rule which is based on D’Alembert’s solution was proposed by John<sup>12</sup> in 1975 and was mainly used to solve the wave problem. The diamond rule has been employed to solve the one-dimensional wave problem of an infinite or a semi-infinite string attached by a mass, spring, or damper<sup>5</sup> and a finite string.<sup>3</sup> Besides, the animation was also given in.<sup>5</sup>

It is necessary to derive the eigenfunctions in advance to obtain the transient response of the bar<sup>13</sup> if the mode superposition approach is considered. Mathematically speaking, the series solution of the dynamic response of the bar can be obtained by using the method of separation variables in conjunction with a truncated series to approximate the real response.<sup>2</sup> The free vibration problem of a finite bar with an external spring has been studied.<sup>14</sup>

<sup>1</sup>Department of Harbor and River Engineering, National Taiwan Ocean University, Keelung, Taiwan

<sup>2</sup>Department of Mechanical and Mechatronic Engineering, National Taiwan Ocean University, Keelung, Taiwan

<sup>3</sup>Ocean Engineering and Technology, National Taiwan Ocean University, Keelung, Taiwan

<sup>4</sup>Department of Civil Engineering, National Cheng Kung University, Tainan, Taiwan

<sup>5</sup>Center of Excellence for Ocean Engineering, National Taiwan Ocean University, Keelung, Taiwan

<sup>6</sup>Department of Civil Engineering, Tamkang University, New Taipei City, Taiwan

## Corresponding author:

Jeng-Tzong Chen, Department of Harbor and River Engineering, National Taiwan Ocean University, No 2, Beining Rd, Zhongzheng Dist., Keelung City 202301, Taiwan (R.O.C.).

Email: [jtchen@mail.ntou.edu.tw](mailto:jtchen@mail.ntou.edu.tw)



Creative Commons CC BY: This article is distributed under the terms of the Creative Commons Attribution 4.0 License (<https://creativecommons.org/licenses/by/4.0/>) which permits any use, reproduction and distribution of the work without further permission provided the original work is attributed as specified on the SAGE and Open Access pages (<https://us.sagepub.com/en-us/nam/open-access-at-sage>).

Besides, the instability is a crucial issue in dynamics. Tian and He<sup>15–19</sup> investigated on the instability of the micro-electromechanical system (MEMS). Nonlinear effect is an interesting and practical issue. In this paper, two methods, the mode superposition method in conjunction with the quasi-static decomposition method and the method of characteristics using the diamond rule, are based on the linear theory. More efforts should be done to extend this approach to nonlinear problem. If transforming a nonlinear PDE to a linear PDE is possible, our approach can be directly applied.

In engineering practice, real cases can be always categorized to two kinds, direct and inverse problems. Regarding the inverse problem, an ill-posed model is always required to be regularized.<sup>20,21</sup> For example, deconvolution of the site response analysis was done by using the Cesàro sum in conjunction with the L-curve.<sup>22,23</sup> Some researchers also solved the inverse problem on vibration problems<sup>24</sup> or the Laplace equation.<sup>25</sup> As shown in Figures 1(a), a finite bar with a spring end (right) subject to the support motion (left) is a direct problem which can be solved by using the well-posed model. On the other hand, in Figure 1(b), the support motion is changed to a free end. If the boundary condition is simultaneously specified for the displacement history and the free traction at the left end, this over-specified boundary condition results in an inverse problem. Therefore, it yields an ill-posed model, although we focus on the support motion of Figure 1(a) only. However, why Figure 1(b) is an ill-posed model can be detected by using the present approach of the diamond rule. For the direct problem of Figure 1(a), the support displacement history,  $a(t)$ , can be arbitrarily specified by the experiment. The unique solution can be obtained and the reaction of axial force history can be correspondingly obtained. However, the arbitrary  $a(t)$  in Figure 1(b) may result in nonzero traction at the free end. This supports that the solution may not exist. Ill-posed model may have three outcomes, nonexistence, non-uniqueness and instability of solution.

The main concern of this paper is to find an efficient way to solve the vibration problem of the finite bar with an external spring on one side and the support motion on the other side. We employ two methods, including the series solution with the quasi-static decomposition method and the method of the diamond rule. Advantages and disadvantages of both methods will be investigated in this paper.

## Problem statements and methods of solutions

We consider a finite bar with an external spring as shown in Figure 1(a). The governing equation for the vibration problem of finite bar is shown below:

$$c^2 \frac{\partial^2 u(x,t)}{\partial x^2} = \frac{\partial^2 u(x,t)}{\partial t^2}, \quad 0 < x < L, \quad t > 0 \quad (1)$$

where  $c = \sqrt{E/\rho}$  and  $u(x,t)$  denote the wave speed and displacement in the  $x$  direction, respectively. The symbols  $E, \rho$  and  $L$  denote Young's modulus, density, and length of the bar, respectively. The initial displacement and velocity conditions are

$$u(x,t)|_{t=0} = \phi(x) = 0 \quad (2)$$

$$\frac{\partial u(x,t)}{\partial t} \Big|_{t=0} = \varphi(x) = 0 \quad (3)$$

where  $\phi(x)$  and  $\varphi(x)$  are initial displacement and velocity functions, respectively.

The boundary condition at the left hand side ( $x = 0$ ) can be expressed by the support motion as follows:

$$u(0,t) = a(t) \quad (4)$$

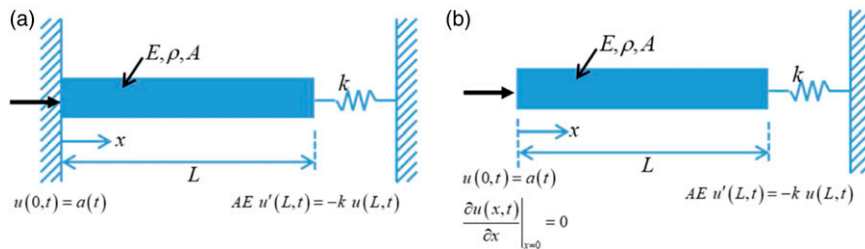


Figure 1. Sketch of the problem.

The boundary condition at the right hand side ( $x = L$ ) is given from the condition of force equilibrium as follows:

$$EA \frac{\partial u(x,t)}{\partial x} \Big|_{x=L} = -ku(x,t) \Big|_{x=L} \quad (5)$$

where  $k$  denotes the spring constant, and  $A$  is the area of cross section.

Equation (1) in conjunction with B.C. of equations (4) and (5) and initial condition of equations (2) and (3) is a well-posed model for the direct problem of support motion at the fixed end instead of the free end.

### *Method 1: Mode superposition in conjunction with the quasi-static decomposition method*

The solution can be decomposed into two parts

$$u(x,t) = U(x,t) + \sum_{n=1}^{\infty} q_n(t)u_n(x) \quad (6)$$

where  $U(x,t)$  denotes the quasi-static solution, and the natural modes  $u_n(x)$  weighted by the generalized coordinate,  $q_n(t)$ , are the dynamic contribution due to the inertia effect. The quasi-static part  $U(x,t)$  satisfies the governing equation

$$EA \frac{\partial^2 U(x,t)}{\partial x^2} = 0, 0 < x < L \quad (7)$$

and is subject to time-dependent boundary conditions:

$$U(0,t) = a(t) \quad (8)$$

$$EA \frac{\partial U(x,t)}{\partial x} \Big|_{x=L} = -kU(x,t) \Big|_{x=L} \quad (9)$$

By solving the PDE in equation (7) with boundary conditions in equations (8) and (9), we have the quasi-static solution.

$$U(x,t) = a(t) \left( 1 - \frac{k}{AE + kL} x \right) \quad (10)$$

The  $n$ th natural mode  $u_n(x)$  satisfy the governing equation

$$u_n''(x) + \lambda_n^2 u_n(x) = 0, n = 1, 2, 3... \quad (11)$$

subject to boundary conditions:

$$u_n(0) = 0 \quad (12)$$

at the fixed end of  $x = 0$ ,

$$EA \frac{\partial u_n(x)}{\partial x} \Big|_{x=L} = ku_n(x) \Big|_{x=L} \quad (13)$$

at the spring end of  $x = L$ .

By solving equation (11) subject to boundary conditions of equations (12) and (13), we have the  $n$ th natural mode  $u_n(x)$  of the eigenvalue  $\lambda_n$

$$u_n(x) = \sin(\lambda_n x), n = 1, 2, 3... \quad (14)$$

where the nonlinear eigenequation is given by

$$\lambda_n = \frac{-k \tan(\lambda_n L)}{AE}, n = 1, 2, 3... \quad (15)$$

and the corresponding natural frequency is

$$\omega_n = \lambda_n \sqrt{E/\rho}, \quad n = 1, 2, 3, \dots \quad (16)$$

The orthogonality of the eigenfunction is

$$\int_0^L u_n(x)u_m(x)dx = \delta_{nm}N_n, \quad n = 1, 2, 3, \dots, m = 1, 2, 3, \dots \quad (17)$$

where  $\delta_{nm}$  is the Kronecker delta and

$$N_n = \frac{L}{2} - \frac{\sin(2\lambda_n L)}{4\lambda_n} \quad (18)$$

Substituting equation (6) into equation (1), we obtain

$$\sum_{n=1}^{\infty} [\ddot{q}_n(t) + \omega_n^2 q_n(t)] u_n(x) = -\ddot{U}(x,t) \quad (19)$$

Multiplying both sides of equation (19) by  $u_m(x)$ , integrating over  $(0,L)$  and applying the orthogonality condition in equation (17), we have  $q_n(t)$  satisfying the following equation

$$\ddot{q}_n(t) + \omega_n^2 q_n(t) = \frac{\ddot{F}_n(t)}{N_n} \quad (20)$$

where

$$F_n(t) = - \int_0^L U(x,t)u_n(x)dx \quad (21)$$

After considering the initial conditions, we have

$$N_n q_n(0) = - \int_0^L U(x,0)u_n(x)dx = F_n(0), \quad (\text{n no sum}) \quad (22)$$

$$N_n \dot{q}_n(0) = - \int_0^L \dot{U}(x,0)u_n(x)dx = \dot{F}_n(0), \quad (\text{n no sum}) \quad (23)$$

Thus, we can solve  $q_n(t)$  by using equations (20), (22), and (23), to obtain

$$q_n(t) = \frac{4[-(AE + kL)\lambda_n + AE \cos(L\lambda_n) + k \sin(L\lambda_n)]}{c(AE + kL)\lambda_n^2[2L\lambda_n - \sin(2L\lambda_n)]} \left[ c\lambda_n a(0)\cos(\lambda_n ct) + \dot{a}(0)\sin(\lambda_n ct) + \int_0^t \sin(\lambda_n c(t - \tau))\ddot{a}(\tau)d\tau \right] \quad (24)$$

Then, the series solution for the displacement,  $u(x,t)$ , and the axial force,  $p(x,t)$ , can be expressed, respectively, as

$$u(x,t) = a(t) \left( 1 - \frac{k}{AE + kL} x \right) + \sum_{n=1}^{\infty} q_n(t) \sin(\lambda_n x) \quad (25)$$

$$p(x,t) = AE \frac{\partial u(x,t)}{\partial x} = AE \left[ \left( \frac{-a(t)k}{AE + kL} \right) + \sum_{n=1}^{\infty} q_n(t) \lambda_n \cos(\lambda_n x) \right] \quad (26)$$

where  $q_n(t)$  is shown in equation (24).

### Method 2: Method of characteristics in conjunction with the diamond rule

By employing the method of characteristic line, we can assume the general solution of 1D wave equation in equation (1) as

$$u(x,t) = P(x + ct) + Q(x - ct) \quad (27)$$

where  $P(x + ct)$  and  $Q(x - ct)$  are specified functions to match initial conditions in equations (2) and (3). The functions  $P(x + ct)$  and  $Q(x - ct)$  represent a left-going-traveling wave and a right-going-traveling wave, respectively. By satisfying equations (2) and (3) for equation (27), the D'Alembert solution is expressed as

$$u(x,t) = \frac{1}{2}[\phi(x + ct) + \phi(x - ct)] + \frac{1}{2c} \int_{x-ct}^{x+ct} \varphi(\tau) d\tau \quad (28)$$

where  $\phi(x)$  and  $\varphi(x)$  are functions of initial displacement and velocity, respectively. Two groups of characteristic lines from equation (28) are included in the solution of the wave equation. Moreover, the two groups of parallel characteristic lines can form a parallelogram in the plane of space-time region as shown in Figure 2. Based on D'Alembert's solution, we have the diamond rule<sup>5</sup>, as shown below

$$u_A + u_B = u_C + u_D \quad (29)$$

where  $u_A, u_B, u_C$  and  $u_D$  denote the displacement at the four points  $A, B, C$ , and  $D$ , respectively. Several characteristic lines separate the domain into many regions as shown in Figure 3. The diagrams of calculating the displacement by using the diamond rule in the regions I, II, III, IV, V, and VI are given in Figure 4. The displacements in the former six regions are given below

$$u_I(x,t) = 0, (x,t) \in I \quad (30)$$

$$u_{II}(x,t) = a\left(\frac{ct-x}{c}\right), (x,t) \in II \quad (31)$$

$$u_{III}(x,t) = r_1\left(\frac{x+ct-L}{c}\right), (x,t) \in III \quad (32)$$

$$u_{IV}(x,t) = a\left(\frac{ct-x}{c}\right), (x,t) \in IV \quad (33)$$

$$u_V(x,t) = a\left(\frac{ct-x}{c}\right), (x,t) \in V \quad (34)$$

$$u_{VI}(x,t) = a\left(\frac{ct-x}{c}\right) - a\left(\frac{x+ct-2L}{c}\right) + r_2\left(\frac{x+ct-L}{c}\right), (x,t) \in VI \quad (35)$$

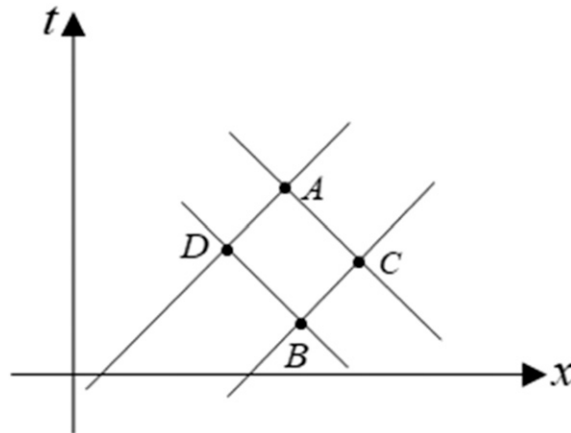


**Figure 2.** The diamond rule of  $u_A + u_B = u_C + u_D$ .

Then,  $r_1(t)$  and  $r_2(t)$  denote the displacements of  $u(L,t)$ ,  $0 \leq t \leq L/c$  and  $u(L,t)$ ,  $L/c \leq t \leq 2L/c$ , which can be obtained from the condition of force equilibrium at  $x = L$

$$EA \frac{\partial u_{III}(x,t)}{\partial x} \Big|_{x=L} = -ku_{III}(x,t) \Big|_{x=L} \quad (36)$$

$$EA \frac{\partial u_{VI}(x,t)}{\partial x} \Big|_{x=L} = -ku_{VI}(x,t) \Big|_{x=L} \quad (37)$$

Thus, we can determine  $r_1(t)$  by using equation (32) to satisfy equation (36). The displacement at  $x = L$ ,  $u_{III}(L,0)$  and  $u_I(L,0)$ , must satisfy the displacement continuity. Then, we have

$$r_1(t) = 0, 0 \leq t \leq \frac{L}{c} \quad (38)$$

Similarly, the response of  $r_2(t)$  can be obtained by using equation (35) to satisfy equation (37). The displacement at

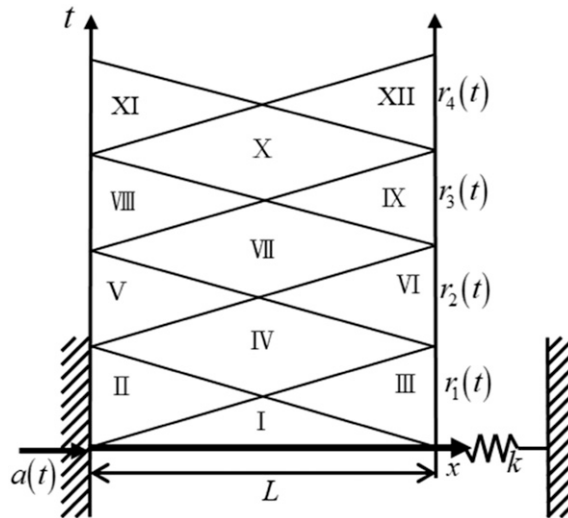


Figure 3. Regions separated by using the characteristic line.

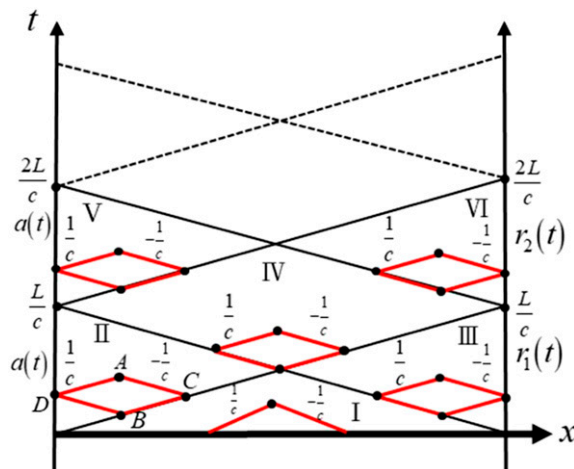


Figure 4. Space-time regions, I, II, III, IV, V, and VI.

$x = L$ ,  $u_{VI}\left(L, L/c\right)$  and  $u_{IV}\left(L, L/c\right)$ , must satisfy the displacement continuity. Then, we have

$$r_2(t) = \frac{\int e^{\frac{kc}{AE}t} 2a'\left(\frac{ct-L}{c}\right) dt}{e^{\frac{kc}{AE}t}}, \frac{L}{c} \leq t \leq \frac{2L}{c} \quad (39)$$

By the same way,  $r_3(t)$  and  $r_4(t)$  can be successively obtained in the space-time marching scheme according to the diamond rule as shown in Figure 3. Responses of  $r_3(t)$  and  $r_4(t)$  are similarly derived as shown below

$$r_3(t) = \frac{\int e^{\frac{kc}{AE}t} 2a'\left(\frac{ct-L}{c}\right) dt}{e^{\frac{kc}{AE}t}}, \frac{2L}{c} \leq t \leq \frac{3L}{c} \quad (40)$$

$$r_4(t) = \frac{\int e^{\frac{kc}{AE}t} \left[ 2a'\left(\frac{ct-L}{c}\right) + 2a'\left(\frac{ct-3L}{c}\right) - 2r_2'\left(\frac{ct-2L}{c}\right) \right] dt}{e^{\frac{kc}{AE}t}}, \frac{3L}{c} \leq t \leq \frac{4L}{c} \quad (41)$$

Regions I and III are called the dead zone due to the fact that the carried information of disturbance does not arrive yet. The space derivative of displacement of each region is shown below

$$u_I'(x,t) = 0, (x,t) \in I \quad (42)$$

$$u_{II}'(x,t) = -\frac{1}{c} a'\left(\frac{ct-x}{c}\right), (x,t) \in II \quad (43)$$

$$u_{III}'(x,t) = \frac{1}{c} r_1'\left(\frac{x+ct-L}{c}\right), (x,t) \in III \quad (44)$$

$$u_{IV}'(x,t) = -\frac{1}{c} a'\left(\frac{ct-x}{c}\right), (x,t) \in IV \quad (45)$$

$$u_V'(x,t) = -\frac{1}{c} a'\left(\frac{ct-x}{c}\right), (x,t) \in V \quad (46)$$

$$u_{VI}'(x,t) = -\frac{1}{c} a'\left(\frac{ct-x}{c}\right) - \frac{1}{c} a'\left(\frac{x+ct-2L}{c}\right) + \frac{1}{c} r_2'\left(\frac{x+ct-L}{c}\right), (x,t) \in VI \quad (47)$$

## An illustrative example

A finite bar with an external spring subjected to a support motion is considered. The model parameters are given as follows:  $c = 1 \text{ m/s}$ ,  $AE = 1\text{N}$ ,  $L = 7\text{m}$  and  $k = 2\text{N/m}$ . By setting the support motion

$$a(t) = \sin(t) \quad (48)$$

the solutions of two approaches can be obtained as shown in the following subsection.

### Mode superposition method

By substituting model parameters  $c, A, E, L, k$  and equation (48) into equations (25) and (26), we have

$$u(x,t) = \sin(t) \left( 1 - \frac{2}{15}x \right) + \sum_{n=1}^{\infty} \left( \frac{4[-15\lambda_n + \lambda_n \cos(7\lambda_n) + 2 \sin(7\lambda_n)] [-\sin(t) + \lambda_n \sin(\lambda_n t)]}{15\lambda_n(-1 + \lambda_n^2)[14\lambda_n - \sin(14\lambda_n)]} \right) \sin(\lambda_n x) \quad (49)$$

$$u'(x,t) = -\frac{2}{15}\sin(t) + \sum_{n=1}^{\infty} \left( \frac{4[-15\lambda_n + \lambda_n \cos(7\lambda_n) + 2 \sin(7\lambda_n)][-\sin(t) + \lambda_n \sin(\lambda_n t)]}{15(-1 + \lambda_n^2)[14\lambda_n - \sin(14\lambda_n)]} \right) \cos(\lambda_n x) \quad (50)$$

Besides, we provide the former six eigenfrequencies and natural modes by using the FEM to compare with analytical results. The comparison is shown in Table 1, good agreement is made.

### Method of the diamond rule

By substituting model parameters  $c, A, E, L, k$  and equation (48) into equations (30)–(35), we have

$$u_I(x,t) = 0, (x,t) \in I \quad (51)$$

$$u_{II}(x,t) = \sin(t-x), (x,t) \in II \quad (52)$$

$$u_{III}(x,t) = 0, (x,t) \in III \quad (53)$$

$$u_{IV}(x,t) = \sin(t-x), (x,t) \in IV \quad (54)$$

$$u_V(x,t) = \sin(t-x), (x,t) \in V \quad (55)$$

$$u(x,t) = \sin(t-x) - \sin(x+t-14) + r_2(x+t-7), (x,t) \in VI \quad (56)$$

where

$$r_2(t) = -\frac{2[-2\cos(7-t) + \sin(7-t)]}{5} - \frac{4}{5}e^{2(7-t)}, 7 \leq t \leq 14 \quad (57)$$

By similarly substituting equation (48) into equations (40) and (41),  $r_3$  and  $r_4$  become

$$r_3(t) = -\frac{2[-2\cos(7-t) + \sin(7-t)]}{5} - \frac{4}{5}e^{2(7-t)}, 14 \leq t \leq 21 \quad (58)$$

$$r_4(t) = \frac{2}{25}e^{-2t}[-10e^{14} + 838e^{42} - 40e^{42}t + 10e^{2t} \cos(7-t) + 2e^{2t} \cos(21-t) - 5e^{2t} \sin(7-t) - 11e^{2t} \sin(21-t)], 21 \leq t \leq 28 \quad (59)$$

The space derivative of displacement of each region is shown below:

$$u_I'(x,t) = 0, (x,t) \in I \quad (60)$$

$$u_{II}'(x,t) = -\cos(t-x), (x,t) \in II \quad (61)$$

$$u_{III}'(x,t) = 0, (x,t) \in III \quad (62)$$

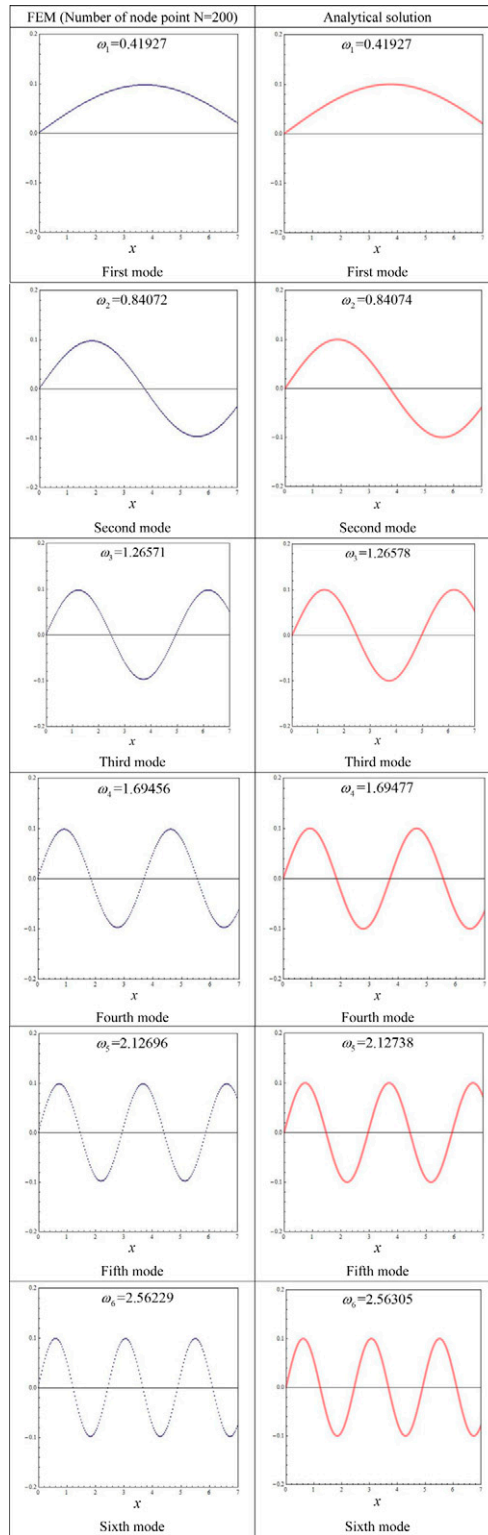
$$u_{IV}'(x,t) = -\cos(t-x), (x,t) \in IV \quad (63)$$

$$u_V'(x,t) = -\cos(t-x), (x,t) \in V \quad (64)$$

$$u_{VI}'(x,t) = -\cos(t-x) - \cos(x+t-14) - \frac{2[-2 \cdot \sin(14-x-t) - \cos(14-x-t)]}{5} + \frac{8}{5}e^{2(14-x-t)}, (x,t) \in VI \quad (65)$$

The displacement profiles with the silent area for  $t = 1, 3,$  and  $5$  s by using the mode superposition method and the diamond rule are shown in Figure 5(a)–(c), respectively. It is interesting to find that the mode superposition method also yields the silent response. In Figure 6, shadow regions, I and III, denote the dead zone. It matches the silent responses begin at  $x = 1, 3,$  and  $5$  m to the end of bar ( $x = 7$  m), for the time when  $t = 1, 3,$  and  $5$  s as shown in Figure 5. It is found that the slopes are discontinuous at  $x = 1, 3,$  and  $5$  m when  $t = 1, 3,$  and  $5$  s, respectively. These discontinuities occur at (1,1), (3,3), and (5,5) in the  $(x-t)$  plane as shown in Figure 6. As theoretically predicted, the discontinuities of the slope really occur at the position of (1,1), (3,3), and (5,5), on the characteristic line.

**Table 1.** The former six eigenfrequencies and eigenmodes by using the analytical solution and the finite element method.



FEM: finite element method.

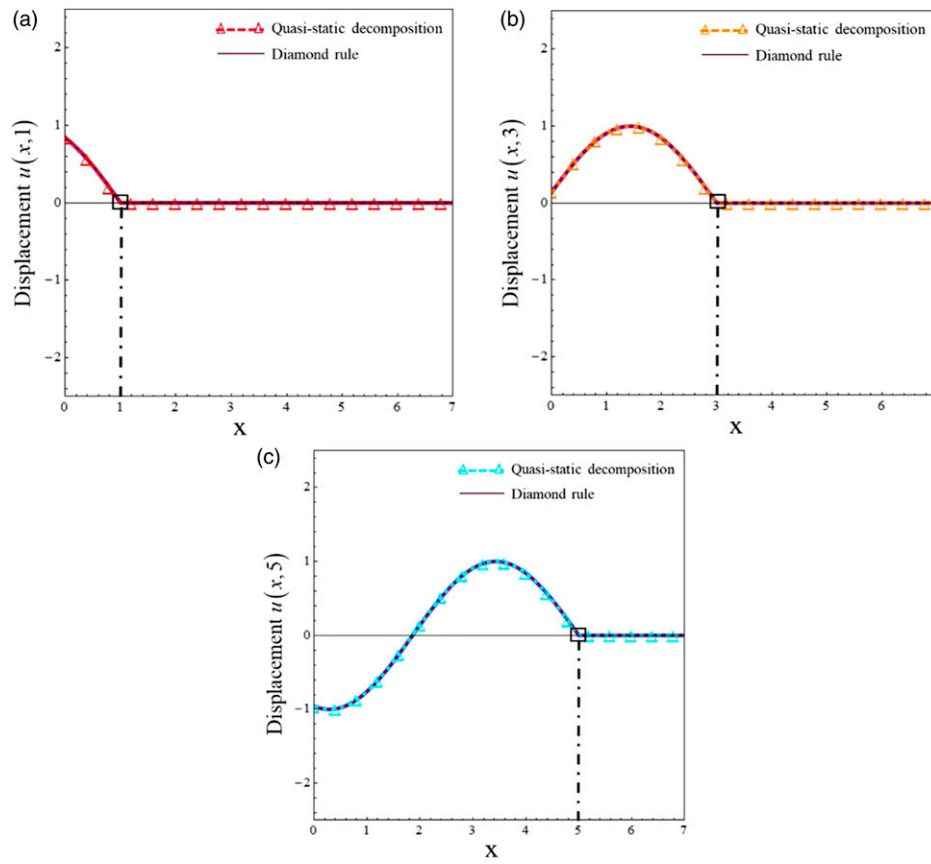


**Figure 5.** Displacement profiles with the silent area by using the quasi-static decomposition and the diamond rule.

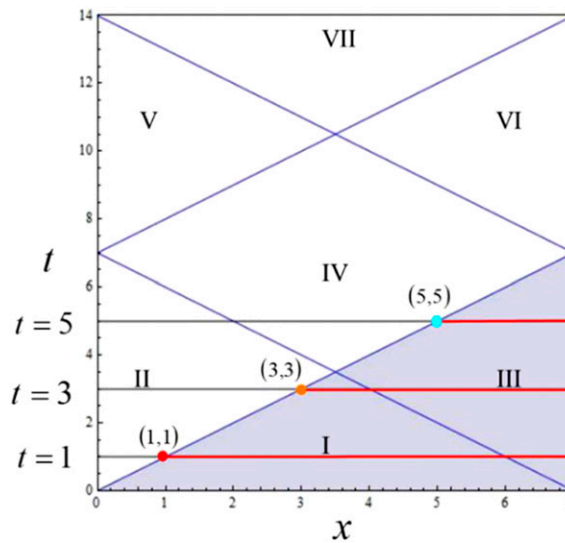


**Figure 6.** The locations of slope discontinuities at (1,1), (3,3), and (5,5), where the shadow region denotes the dead zone.

Regarding no silent area, the displacement profiles at  $t = 7, 9,$  and  $11$  s are shown in [Figure 7\(a\)-\(c\)](#), respectively. It is also found that the slope is discontinuous at  $x = 5$  and  $3$  m when  $t = 9$  and  $11$  s, respectively. These slope discontinuities occur at locations of (5,9) and (3,11) in the  $x-t$  plane as shown in [Figure 8](#). This finding matches well from the mathematical requirement that the discontinuity must occur at the position on the characteristic line<sup>26</sup>.

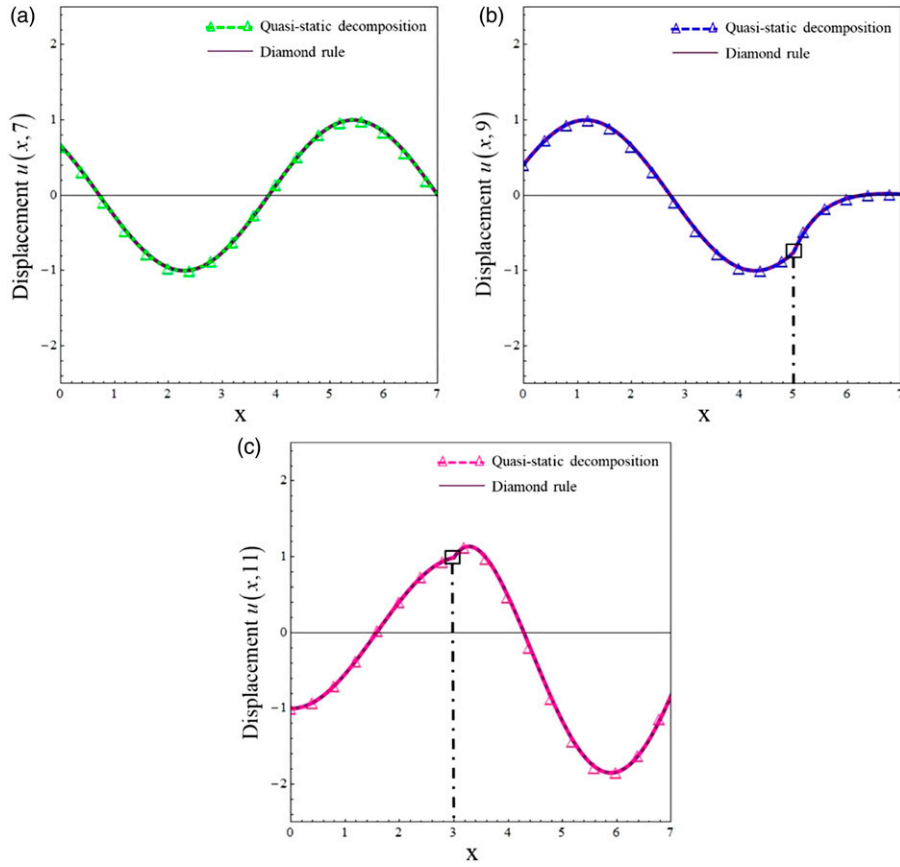


Figure 7. Displacement profiles without the silent area by using the quasi-static decomposition and the diamond rule

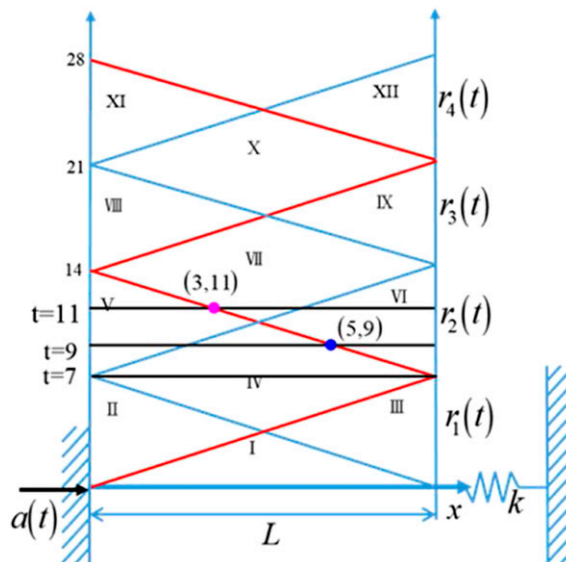
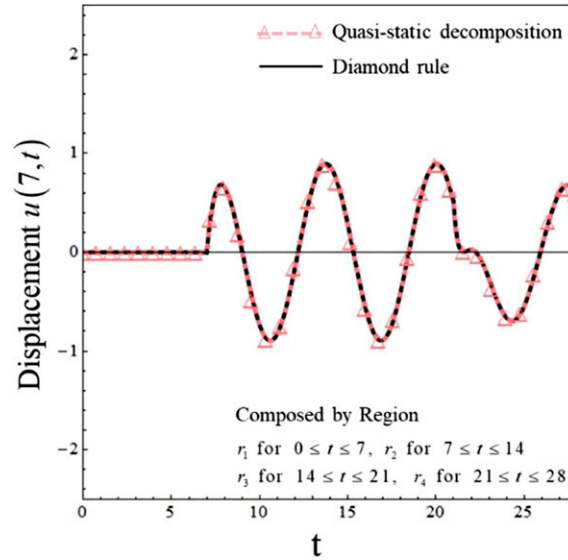
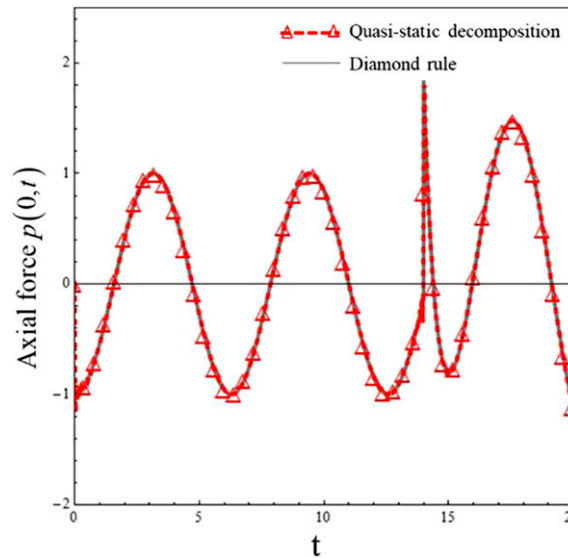


Figure 8. The locations of slope discontinuities at (3,11) and (5,9).



**Figure 9.** Displacement history at  $x = 7$  m.



**Figure 10.** History of the axial force at  $x = 0$  m (fixed end) by using the mode superposition method and the diamond rule.

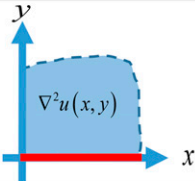
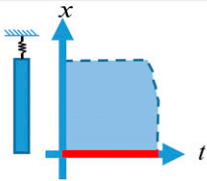
In order to ensure the convergence of series solution, the displacement profiles using 5, 10, 25, 50, and 100 modes are shown in Table 2. Here, we adopt the solution of diamond rule in the IV region ( $t = 7$ ) for simplicity.

The displacement response at  $x = 7$  m by using the mode superposition method and the diamond rule are shown in Figure 9. The axial force of reaction at  $x = 0$  m by using the mode superposition method and the diamond rule are shown together in Figure 10. It is interesting to find that the axial force has an impulse at  $t = 14$  s. Besides, the axial force is not zero at the beginning ( $t = 0$ ) subjected to the support motion at the left end of the finite bar. According to Figure 10, it indicates that there is a reaction force history to have a support motion of  $a(t)$ . Therefore, a specified displacement history,  $a(t)$ , at the free end,  $x = 0$ , is an inverse problem. A comparison for the ill-posed model between the statics (Laplace equation) and dynamics (wave equation) is given in Table 3. Both cases show the similar over-specified conditions.

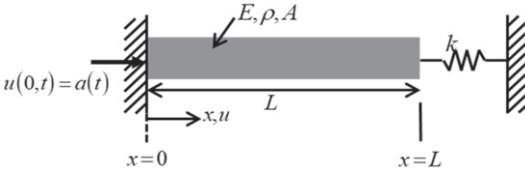
**Table 2.** Convergence of the displacement profiles at  $t = 7$  sec for the solution in the region IV by using the quasi-static decomposition and the error plot.

<p>(a) <math>M=5</math>, Error <math>\approx 0.0179139</math></p>	<p>(b) <math>M=10</math>, Error <math>\approx 0.00207871</math></p>
<p>(c) <math>M=25</math>, Error <math>\approx 0.000152569</math></p>	<p>(d) <math>M=50</math>, Error <math>\approx 0.0000221562</math></p>
<p>(e) <math>M=100</math>, Error <math>\approx 5.82354 \cdot 10^{-6}</math></p>	<p>(f) Error plot</p>
<p>Note:</p> $\text{Error} = \int_0^7 \left\{ \left[ \sin(t) \left( 1 - \frac{2}{15}x \right) + \sum_{n=1}^M \left( \frac{4[-15\lambda_n + \lambda_n \cos(7\lambda_n) + 2\sin(7\lambda_n)] [-\sin(t) + \lambda_n \sin(\lambda_n t)]}{15\lambda_n(-1 + \lambda_n^2) [14\lambda_n - \sin(14\lambda_n)]} \sin(\lambda_n x) \right) \right] \sin(\lambda_n x) \right\}^2 dx \Bigg _{t=7}$	

**Table 3.** Comparison of ill-posed models in statics and dynamics.

Laplace equation (statics)	Wave equation (dynamics)
Hadamard [22]	Present study
 $\frac{\partial^2 u(x,y)}{\partial x^2} + \frac{\partial^2 u(x,y)}{\partial y^2} = 0$	 $c^2 \frac{\partial^2 u(x,t)}{\partial x^2} = \frac{\partial^2 u(x,t)}{\partial t^2}$
 $u(x,0) = 0$ $u_y(x,0) = \frac{1}{n} \sin(nx)$	 $u(0,t) = a(t)$ $u_x(0,t) = 0$
$u(x,y) = \frac{1}{n^2} \sin(nx) \sinh(ny) \Rightarrow n \rightarrow \infty \Rightarrow u(x,y) \rightarrow \infty$	$u(x,t) = ?$
Ill-posed model	Ill-posed model ?

**Table 4.** Comparison of the both approaches for the vibration problem of a finite rod.

		
Method	Mode superposition method in conjunction with the quasi-static decomposition	Method of characteristics in conjunction with the diamond rule
Item analysis		
Solution form	Series solution (continuous)	Exact solution (continuous)
Advantage	Without dividing the space-time region to represent the corresponding displacement response	1. Without the truncation error of finite term of series sum 2. It can analytically capture the dead zone
Disadvantage	Error due to truncation series in the real computation	Previous stage error propagates to the later response

## Discussions

We must carefully derive the solution because the wrong data at the previous stage deteriorate the later response when the space-time region is marching in the scheme of the diamond rule. The dead zone and silent response can be both analytically and numerically captured by using the mode superposition technique and the method of characteristics, respectively. The slope discontinuity is also observed at the position  $(x, t)$  on the characteristic lines. Two analytical approaches yield agreeable numerical results. Gibbs phenomenon is also observed for the axial force at  $t = 0$  obtained by using the mode superposition method. Table 4 summarizes the comparison of the two approaches.

If the same  $a(t)$  is given in Figure 1(b) (inverse problem), the identical solution is obtained by using the diamond rule. However, this result contradicts the zero axial force at the free end. From the experiment point of view,  $a(t)$  in Figure 1 can be arbitrarily specified to yield the corresponding reaction force. That is to say,  $a(t)$  in Figure 1(b) should satisfy some consistent constraint. Table 3 also shows the ill-posed model for statics and dynamics.

## Conclusions

In this paper, we have successfully solved the direct problem of the longitudinal vibration analysis of a finite bar with an external spring on one side and the support motion on the other fixed side by using two methods. The inverse problem was also discussed. Both approaches can analytically and numerically capture the silent response by using the mode superposition method and the method of characteristics, respectively. The slope discontinuity occurs at the position on the characteristic line as mathematically predicted. Two results show that good agreement is made. The solution by using the diamond rule depends on the previous result of the space-time region and the error is accumulated. However, the mode superposition method has the truncation error due to the finite term of series sum. Convergence study was also done. Finally, the advantage and disadvantage for two methods were summarized in Table 4.

## Declaration of Conflicting Interests

The author(s) declared no potential conflicts of interest with respect to the research, authorship, and/or publication of this article.

## Funding

The author(s) disclosed receipt of the following financial support for the research, authorship, and/or publication of this article: Financial support from the Ministry of Science and Technology under Grant No. 110-2813-C-019-063-E and the Grant No. 110-2813-C-019-063-E for the undergraduate student H. C. Kao, for the National Taiwan Ocean University is gratefully acknowledged.

## ORCID iD

Jeng-Tzong Chen  <https://orcid.org/0000-0001-5653-5061>

## References

1. Oliveto G, Santini A, and Tripodi E. Complex modal analysis of a flexural vibrating beam with viscous end conditions. *J Sound Vib* 1997; 200: 327–345.
2. Hull AJ. A closed form solution of a longitudinal bar with a viscous boundary condition. *J Sound Vib* 1994; 169: 19–28.
3. Chen JT and Jeng YS. Dual series representation and its applications to a string subjected to support motions. *Adv Eng Softw* 1996; 27: 227–238.
4. Chen JT, Hong H-K, Yeh CS, et al. Integral representations and regularizations for a divergent series solution of a beam subjected to support motions. *Earthquake Eng Struct Dyn* 1996; 25: 909–925.
5. Chen JT, Chou KS, and Kao SK. One-dimensional wave animation using mathematica. *Comp Appl Eng Edu* 2009; 17: 323–339.
6. Zhao L and Chen Q. Neumann dynamic stochastic finite element method of vibration for structures with stochastic parameters to random excitation. *Comput Struct* 2000; 77: 651–657.
7. Albuquerque EL, Sollero P, and Fedelinski P. Free vibration analysis of anisotropic material structures using the boundary element method. *Eng Anal Boundary Elem* 2003; 27: 977–985.
8. Li H, Wang QX, and Lam KY. Development of a novel meshless Local Kriging (LoKriging) method for structural dynamic analysis. *Comp Methods Appl Mech Eng* 2004; 193: 2599–2619.
9. Mindlin RD and Goodman LE. Beam vibrations with time-dependent boundary conditions. *J Appl Mech* 1950; 17: 377–380.
10. Farlow SJ. *Partial Differential Equations for Scientists and Engineers*. 1st ed. Canada: John Wiley & Sons, 1937.

11. Wilkinson DH and Curtis EM. *Water Hammer in a Thin Walled Pipe, Proc.* 3rd ed. UK: Int Conf on Pressure Surges, Canterbury, 1980. 221–240.
12. John F. *Partial Differential Equation.* 2th ed. New York: Springer-Verlag, 1975.
13. Tan CA and Ying S. Dynamic analysis of the axially moving string based on wave propagation. *J Appl Mech* 1997; 64: 394–400.
14. Hsu YH, Lee JW, Lee YT, et al. Free vibration analysis of a finite bar with an external spring. In The 34th National Conference on Theoretical and Applied Mechanics, National Yunlin University of Science and Technology, Taiwan, 19-20 November 2010.
15. Tian D, Ain QT, Anjum N, et al. Fractal N/MEMS: form pull-in instability to pull-in stability. *Fractals* 2021; 29(2): 2150030.
16. Tian D, He C-H, and He J-H. Fractal pull-in stability theory for microelectromechanical systems. *Front Phys* 2021; 9: 606011.
17. He J-H, Moatimid GM, and Sayed A. Nonlinear EHD instability of two-superposed walters' b fluids moving through porous media. *Axioms* 2021; 10(4): 258.
18. He JH, Moatimid GM, and Mostapha DR. Nonlinear instability of two streaming-superposed magnetic Reiner-Rivlin Fluids by He-Laplace method. *J Electroanal Chem* 2021: 895: 115388.
19. He J-H, Amer TS, Elnaggar S, et al. Periodic property and instability of a rotating pendulum system. *Axioms* 2021; 10(3): 191.
20. Hadamard J. *Lectures on Cauchy's Problem in Linear Partial Differential Equations.* 1st ed. New York: Dover Publications, 1952.
21. Tikhonov AN, Goncharsky AV, Stepanov VV, et al. *Numerical Methods for the Solution of Ill-Posed Problems.* Boston: Kluwer Academic Publishers, 1995.
22. Hansen PC. Analysis of discrete Ill-posed problems by means of the L-Curve. *SIAM Rev* 1992; 34(4): 561–580.
23. Chen LY, Chen JT, Hong H-K, et al. Application of Cesàro mean and the L-curve for the deconvolution problem. *Soil Dyn Earthquake Eng* 1995; 14: 361–373.
24. Starel L, Inman DJ, and Kress A. A symmetric inverse vibration problem. *J Vib Acoust* 1992; 144(4): 564–568.
25. Chen JT and Chen KH. Analytical study and numerical experiments for Laplace equation with overspecified boundary conditions. *Appl Math Model* 1998; 22: 703–725.
26. Carrier GF and Pearson CE. *Partial Differential Equations: Theory and Technique.* 1st ed. New York: Academic Press, 1976.